

DNA-Directed Assembly of a Cell-Responsive Biohybrid Interface for Cargo Release

Pengchao Sun, Tim Scharnweber, Parvesh Wadhvani, Kersten S. Rabe, and Christof M. Niemeyer*

The development of a DNA-based cell-responsive biohybrid interface that can be used for spatially confined release of molecular cargo is reported. To this end, tailored DNA–protein conjugates are designed as gatekeepers that can be specifically cleaved by matrix metalloproteases (MMPs), which are secreted by many cancer cells. These gatekeepers can be installed by DNA hybridization on the surface of mesoporous silica nanoparticles (MSNs). The MSNs display another orthogonal DNA oligonucleotide that can be exploited for site-selective immobilization on solid glass surfaces to yield micropatterned substrates for cell adhesion. Using the human fibrosarcoma cell line HT1080 that secretes MMPs, it is demonstrated that the biohybrid surface is specifically modified by the cells to release both MSN-bound gatekeeper proteins and the encapsulated cargo peptide KLA. In view of the enormously high modularity of the system presented here, this approach promising for applications in drug delivery, tissue engineering, or other areas of nanobiotechnology is considered.

roughness, there is great interest in generic approaches that can be used to develop adaptive and responsive material systems, which in turn can be used for applications in biomedicine and biotechnology, such as tissue engineering^[2] or stem cell cultivation.^[3] In this context, hybrid material systems whose surface is decorated with nanoparticles allow a wide range of variations, since both the solid bulk phase and the surface can be tailored to adapt both the mechanical and bioinstructive properties to specific needs. As an example, silica nanoparticles (SiNPs), assembled on flat surfaces by nonspecific interactions, were found to substantially affect the spreading, shape, cytoskeletal F-actin alignment, and recruitment of focal adhesion complexes in endothelial cells and preosteoblasts,

1. Introduction

The investigation of interactions between cells and synthetic material surfaces plays a crucial role in the life sciences to understand basic principles of cell adhesion, proliferation, differentiation, and gene expression.^[1] Since cellular behavior is influenced by surface properties such as topography, elasticity, and

presumably due to particle size-dependent changes in the nano-roughness of the surface.^[4] Likewise, densely packed layers of physisorbed SiNPs were found to mediate the developmental acceleration of hippocampal neurons.^[5]

To make this bottom-up approach for the production of functional cell culture substrates more efficient and flexible, so that even complex particulate architectures can be created in a controlled manner on surfaces, we have recently developed the DNA-directed immobilization of SiNPs on glass surfaces. Both solid^[6] and mesoporous^[7] SiNPs could be assembled into well-defined surface-bound patterns of micrometer dimensions. The resulting DNA-decorated SiNP surfaces are highly attractive to living cells, which quickly adhere to the particle-decorated micropatterns. In analogy to the well-known phenomenon that stone pebbles on the sea floor attract marine organisms, we have dubbed this surface structuring the “biopebbles” concept. Since the particles can be chemically encoded with arbitrary dyes, the DNA linkers in between the surface and the nanoparticle can be designed as stable or cleavable, and mesoporous SiNPs (MSNs) can be used for encapsulation of cell-instructive cargo, the biopebble approach can be exploited to investigate basic principles of cell uptake, cell adhesion, and cell guidance with micropatterned surfaces.^[6,7]

Recently, we showed that surface-bound MSNs can be functionalized with an adenosine triphosphate (ATP)-switchable aptamer to respond to global stimuli such as high concentrations of ATP or reducing agents in cell culture medium and release an encapsulated cargo.^[7] However, the switchability of particles by such global parameters is not suitable for achieving responsiveness by local changes with high spatial resolution,

Dr. P. Sun, Dr. T. Scharnweber, Dr. K. S. Rabe, Prof. C. M. Niemeyer
Institute for Biological Interfaces (IBG 1)
Karlsruhe Institute of Technology (KIT)
Hermann-von-Helmholtz-Platz-1, D-76344 Eggenstein-Leopoldshafen
Germany
E-mail: niemeyer@kit.edu

Dr. P. Sun
School of Pharmaceutical Sciences
Zhengzhou University
No.100 Science Avenue, Zhengzhou 450001, China

Dr. P. Wadhvani
Institute for Biological Interfaces (IBG 2)
Karlsruhe Institute of Technology (KIT)
Hermann-von-Helmholtz-Platz-1, D-76344 Eggenstein-Leopoldshafen
Germany

 The ORCID identification number(s) for the author(s) of this article can be found under <https://doi.org/10.1002/smt.202001049>.

© 2021 The Authors. Small Methods published by Wiley-VCH GmbH. This is an open access article under the terms of the Creative Commons Attribution-NonCommercial-NoDerivs License, which permits use and distribution in any medium, provided the original work is properly cited, the use is non-commercial and no modifications or adaptations are made.

DOI: 10.1002/smt.202001049

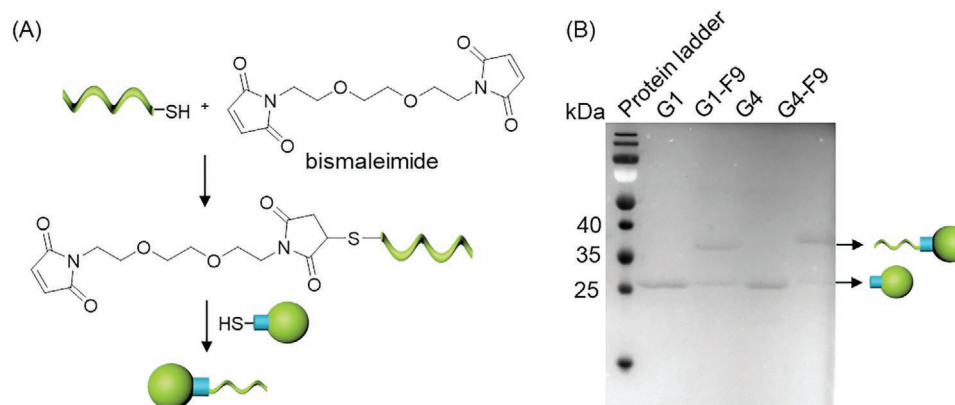


Figure 1. Synthesis and characterization of DNA–protein gatekeeper conjugate. A) Schematic illustration of the synthesis of DNA–protein conjugate via bismaleimide cross-linking. B) 16% SDS-PAGE analysis of DNA–protein gatekeeper conjugates with Coomassie blue staining.

for example, to specifically investigate secretion or uptake of proteins for individual cells. To design and implement responsive gatekeeper systems that are selectively switched by a stimulus released from single cells, we report here the development of a modular supramolecular surface architecture based on novel DNA–protein conjugates that can respond to internal cell stimuli to control the release of encapsulated cargo from MSNs. To this end, we designed a novel class of DNA–protein conjugate that is specifically cleavable by matrix metalloproteases (MMPs), which are secreted by many cancer cells. The DNA–protein conjugate was installed as gatekeeper on DNA-functionalized MSN containers by using one of two orthogonal DNA sequences on the MSN (Figure 1), and the resulting constructs were then assembled on a glass surface to yield microstructured substrates for cell adhesion. Using the human fibrosarcoma cell line HT1080 that secretes MMPs, we demonstrate that the biohybrid surface can be specifically modified by the cells to release particle-bound proteins and low molecular weight cargo.

2. Results and Discussion

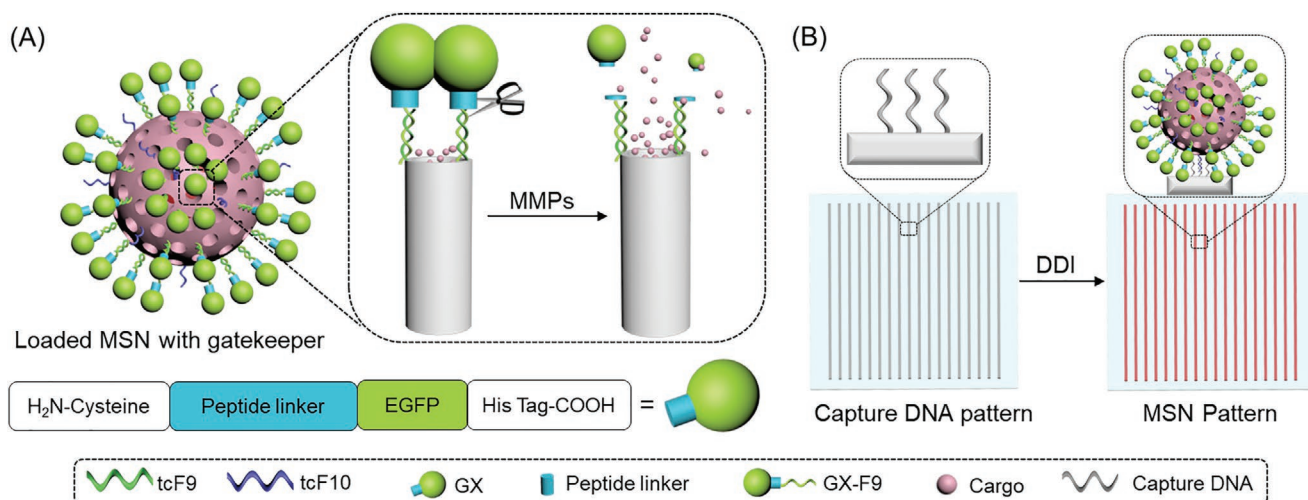
To approach the development of the DNA-controlled assembly of a cell-switchable biohybrid interface, we selected MMPs as triggers with which cells can modify the surface. MMPs are calcium-dependent, zinc-containing endopeptidases, which play a crucial role in cancer development.^[8] They are overexpressed and secreted by many cancer cell lines, such as HT1080 (human, fibrosarcoma), MDA-MB-435 (human, breast cancer), and HT29 (human, colorectal adenocarcinoma) cells,^[9] and owing to their relatively high concentration in the tumor micro-environment, MMPs, especially the family members MMP-2/-9/-14, have already been used as targets for drug delivery.^[10] To design a modular gatekeeper system, a MMP cleavable peptide should be genetically fused with a bulky, traceable protein and we selected the enhanced green fluorescent protein (EGFP) for this purpose. The resulting fusion protein should be conjugated with a DNA oligonucleotide to allow immobilization on the particle surface by DNA hybridization. For this purpose, bifunctional MSNs were used that contained two different

orthogonally addressable DNA oligonucleotides. One of the two sequences should be used for installing the gatekeeper, whereas the other should be used for DNA-directed immobilization of the MSN on DNA-patterned glass surfaces (Scheme 1).

2.1. Synthesis of DNA–Protein Gatekeeper Conjugates

To synthesize the desired MMP-sensitive DNA–protein gatekeeper conjugate, we initially selected peptide sequences known to be specifically cleaved by MMPs (Table S1, Supporting Information). Since various cleavage sites are reported in the literature for MMP-2, -9, or -14, we designed expression plasmids for four different MMP–EGFP variants, in the following text denoted as gatekeeper (GX) variants, in which X indicates a MMP-2/-9 cleave site (G1, G2), a MMP-14 cleavage site (G3), or an uncleavable linker (G4), respectively (Table S1; for sequences of the primers for plasmid construction, see Table S2 in the Supporting Information). The MMP cleavage site was appended to the N-terminus of EGFP and additionally supplemented with an N-terminal Cys residue to enable the site-selective chemical conjugation of DNA oligonucleotides (Scheme 1A). Construction of plasmids was confirmed by agarose gel electrophoresis and the GX variants were expressed in BL21DE3 competent *Escherichia coli* cells and purified by nickel nitrilotriacetic acid affinity chromatography using a fast protein liquid chromatography instrument (Figure S1, Supporting Information), as previously described.^[11] As confirmed by sodium dodecyl sulfate-polyacrylamide gel electrophoresis (SDS-PAGE) analysis, the GX protein variants were successfully purified to near homogeneity and showed the expected molecular weight of ≈ 28 kDa (Figure S2, Supporting Information). Characterization by UV-vis and fluorescence spectroscopy confirmed that the GX variants exhibit the same optical properties as wild-type EGFP (Figure S3, Supporting Information).

The resulting GX variants were then chemically conjugated to a DNA oligonucleotide to obtain DNA–protein gatekeeper conjugates. The linker DNA length could affect the loading efficiency of the MSN, as a longer oligonucleotide would increase the distance between the gatekeeper and the mesopore, which could lead to leakage of the encapsulated cargo. By contrast,



Scheme 1. Schematic illustration of MSNs bearing DNA–protein conjugates as A) a proteinase-responsive gatekeeper and B) the DNA-directed immobilization (DDI) of MSNs. Note that the gatekeeper is bound on the MSN surface by one of two orthogonal DNA sequences (green), while the other (blue) one can be used for DDI of the MSN construct on surfaces patterned with complementary capture oligonucleotides. The scheme below (A) indicates the design of the recombinant gatekeeper protein.

shorter oligonucleotides could cause insufficiently stable attachment of the bulky protein to the MSN surface or even limited steric accessibility for the MMP. Since MMPs have typical sizes of about 4 nm in diameter,^[12] the 22-mer oligonucleotide tF9 was used, which has a nominal length of about 7.5 nm and was modified with a 5'-thiol group for chemical coupling (for DNA sequences, see Table S3 in the Supporting Information).

For the synthesis of the desired GX–F9 conjugate, the bismaleimide cross-linker (1,8-bismaleimido-diethyleneglycol) was initially tested, often used to establish intramolecular thiol–thiol couplings in proteins.^[13] However, we found that it was impossible to purify the desired maleimide-activated GX proteins prior to addition of the thiolated DNA. Even at large excess of 100 equivalents of the cross-linker, very low amounts of the desired GX–F9 conjugates were obtained, suggesting that intermolecular protein cross-coupling occurred as a dominant side reaction (Figure S4, Supporting Information). As an alternative conjugation approach, oligonucleotide tF9 was initially activated with an excess of the bismaleimide, followed by spin column purification and addition of the GX protein to enable the second thiol–maleimide coupling (Figure 1A). We found that a large excess of cross-linker (100 eq) is inevitable to avoid oligonucleotide dimerization (Figure S5, Supporting Information) and 10 eq of maleimide-activated oligonucleotides lead to optimal results (Figure S6, Supporting Information). Under these conditions, the desired DNA–GX conjugates could be obtained in high yields of ≈33%, which was greater than the yields obtained in an alternative cross-linking approach based on the hetero-bispecific cross-linker sulfosuccinimidyl 4-(*N*-maleimidomethyl)cyclohexane-1-carboxylate and amino-derivatized oligonucleotides (≈12% yields, see Figures S7 and S8 in the Supporting Information).

Due to the similar structure of the GX variants, all DNA–protein gatekeeper conjugates (GX–F9) were synthesized by using the above-described methodology. The resulting GX–F9 conjugates were then purified by anion exchange chromatography^[11,14] (Figures S9 and S10, Supporting Information) and further characterized by SDS-PAGE, UV–vis spectroscopy, and

fluorescence spectroscopy, respectively. As shown in Figure 1B and Figure S11 (Supporting Information), the GX–F9 conjugates exhibited a reduced electrophoretic mobility, as compared to the smaller GX variants. The GX–F9 had a molecular weight of ≈38 kDa, as determined by SDS-PAGE, which corresponds to the expected value. Furthermore, the GX–F9 conjugates were capable of hybridization with their complementary oligonucleotide cF9 (Figure S12, Supporting Information). In agreement with previous studies,^[11] the binding of the complementary oligonucleotide did not affect the specific UV–vis absorbance and emission spectra of the fluorescent protein (Figure S13, Supporting Information). The concentration of the GX–F9 conjugates was calculated using calibration samples containing GX and F9 mixed at an equimolar ratio of 1:1.

2.2. Protease-Mediated Cleavage of the DNA–Protein Gatekeeper Conjugates

We then investigated whether the designed DNA–protein gatekeeper conjugate can be cleaved from a solid surface by MMPs. To simplify the analytical method, streptavidin-coated magnetic beads were used as the solid substrate (Figure 2A) onto which the biotin-labeled complementary oligomer bcF9 was immobilized. Following that, the so-prepared beads were used for capturing of the GX–F9 conjugates. Quantitative analysis indicated that ≈70% of immobilized bcF9 was capable of binding the DNA–protein conjugates (Table S4, Supporting Information). To investigate the proteolytic cleavage of GX–F9 conjugates, and, thus, the functionality of the gatekeeper, we applied the collagenase type IV reagent as a model since this reagent is a mixture of MMPs including MMP-2 and MMP-9.^[15]

Subsequent to the addition of collagenase IV to the bead suspension, the fluorescence intensity of the cleaved GX in the supernatant was determined at regular time intervals. As shown in Figure 2B and Figure S14 (Supporting Information), the conjugates G1–F9, G2–F9, and G3–F9 were cleaved off by

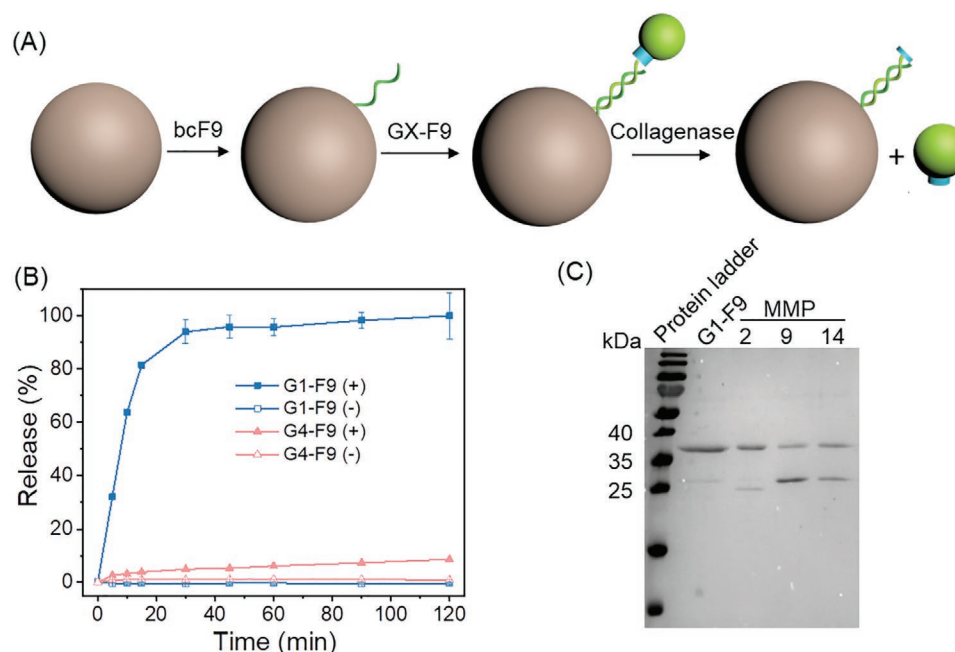


Figure 2. Release of DNA–protein gatekeeper conjugate from magnetic microbeads. A) Schematic illustration for the workflow of the assay. B) Time-dependent collagenase-type-IV-mediated release of the GX–F9 conjugates, as determined by fluorescence analysis of the supernatant in either the presence (+) or absence (–) of collagenase IV. C) SDS-PAGE analysis of MMP-2, -9, -14 mediated hydrolysis of G1–F9. For similar investigations of the G2–F9 and G3–F9 conjugates, see Figure S14 in the Supporting Information.

collagenase IV, whereas experiments with G4–F9 showed no substantial release. We found that G1 and G3 were completely cleaved from the beads within 2 h, whereas only 80% of G2 was released, indicating that the peptide linker sequence of G2 is not equally well cleaved by the enzymes in the collagenase IV cocktail (Figure S14, Supporting Information). Since G1 showed the fastest cleavage kinetics and G4 proved to be a good negative control as expected, these two conjugates were used for further studies. To further examine the sensitivity of G1–F9 against individual MMPs, this conjugate was also incubated with pure MMP-2, -9, and -14, respectively. SDS-PAGE analysis showed that about 20% of G1 was released by MMP-2, whereas more than 50% of G1 was released by treatment with MMP-9 and MMP-14, as determined by grayscale analysis (Figure 2C). The less efficient cleavage of G1–F9 by the MMP-2 might be due to the lower activity of this enzyme, which was also confirmed in control experiments with a commercial peptide substrate (Figure S15, Supporting Information).

2.3. Installment of the DNA–Protein Gatekeeper on DNA-Functionalized MSNs

To install the DNA–protein gatekeeper conjugate on MSNs, bifunctional DNA–MSNs were synthesized following a previously established method, which yields MSNs with average pore sizes of 5.1 nm.^[7] It is known that the size and density of mesopores, often referred to as pore volume, determine the size of the cargo and its loading capacity in MSNs and can be varied by alternative methods of colloidal synthesis.^[16] To produce the MSN used here, thiol-functionalized MSN-1 was first prepared

by cocondensation of (3-mercaptopropyl)trimethoxysilanes. This procedure also allowed to incorporate fluorescent Cy5 or Cy3 dyes as internal labels.^[6] The obtained MSNs were characterized by transmission electron microscopy (TEM, see Figure S16 in the Supporting Information) and dynamic light scattering (DLS, see Table S5 in the Supporting Information). DLS measurements revealed that MSN-1 was monodispersed in water (polydispersity index < 0.1) with a hydrodynamic size of ≈ 113 nm, which is bigger than the TEM size (97 ± 6 nm). The amount of thiol groups on the particle surface was found to be about $256 \mu\text{mol g}^{-1}$, as determined by Ellman's assay. Modification with two orthogonal DNA oligonucleotides was achieved in two consecutive steps (Figure 3). The thiol groups on the MSN surface were initially activated with 2,2'-dithiodipyridine (DTDP) to yield MSN-2. These particles were then allowed to bind a first thiolated oligomer (tcF9, MSN-3) followed by brief washing and coupling of the second oligomer (tcF10) to yield MSN-4.

Quantification of the amounts of oligonucleotides bound to the MSN indicated that the amount of the first applied oligomer (tcF9) was larger than that of the second applied oligonucleotide tcF10 (Table S5, Supporting Information). However, the amounts of tcF10 were still sufficient to facilitate the surface assembly of the particles (see below). The resulting particles MSN-4 were then allowed to bind GX–F9 to yield mesopore-capped MSN-5 (Figure 3). Determination of an increased hydrodynamic size, variation in the zeta potential, and changes in the density of functional groups (Table S5, Supporting Information) indicated the successful installment of the gatekeeper. The successful hybridization of G1–F9 onto the MSN-5 particles was also confirmed by fluorescence spectroscopy (Figure 4A), where the emission spectrum showed a clear peak at 510 nm, which is

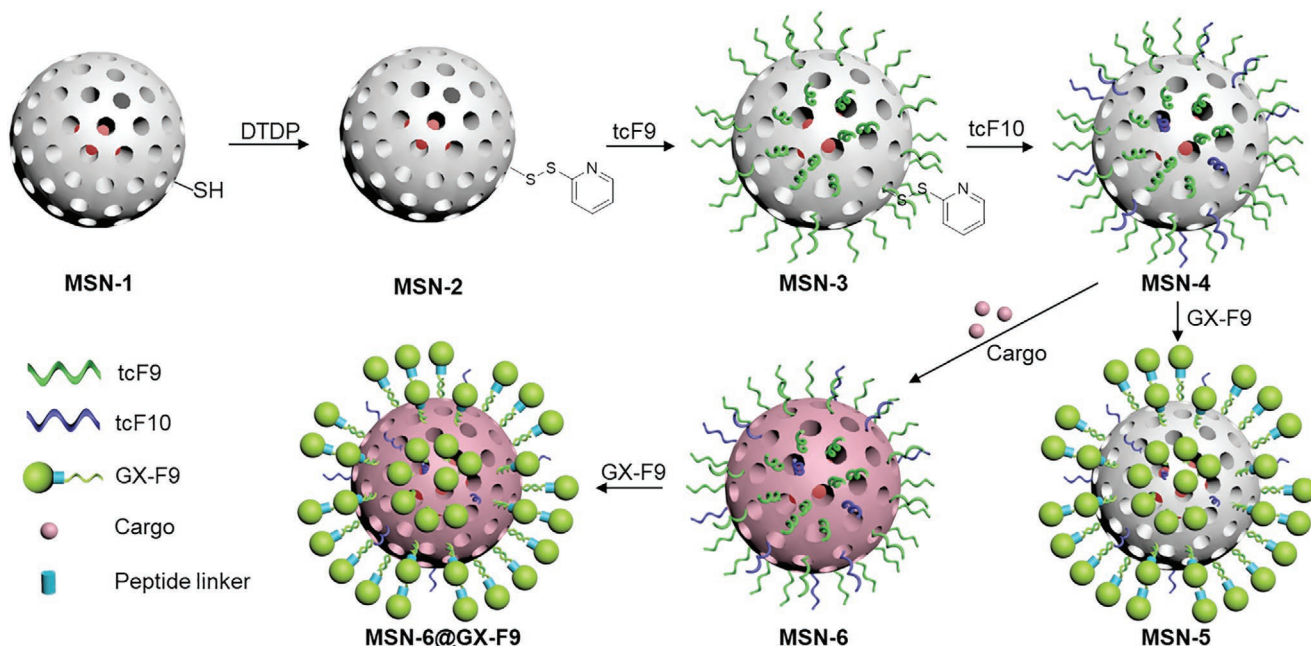


Figure 3. Schematic illustration of the synthesis of DNA–protein-gatekeeper-functionalized MSNs. All MSN particles contained internal Cy5 labels. Note that MSN-4 particles are bifunctional due to the presence of two orthogonal DNA sequences (cF9, cF10), one of which can be used for installation of the gatekeeper whereas the other one can be used for DNA-directed immobilization on glass surfaces patterned with complementary capture oligonucleotides.

indicative for the EGFP emission. Furthermore, the presence of G1–F9 on the MSN-5 surface was proven by SDS-PAGE analysis of the constructs, where the appearance of a band at ≈ 38 kDa indicated the presence of G1–F9 (lane 3, in Figure 4B). It could be shown that G1 was released from the particle surface after the treatment of MSN-5 with collagenase type IV (lane 8).

Since HT1080 cells are known for high overexpression of MMPs,^[17] we selected this cell line as the model for the MMP-responsive studies. Therefore, a conditioned medium from HT1080 cells was also tested, whether sufficient amounts of MMPs were secreted to cleave G1–F9 from MSN-5 (Figure S17, Supporting Information). As indicated by western blot analysis, the presence of uncleaved G1–F9 suggested that the

concentration of MMPs secreted by HT1080 cells is not sufficiently high in the medium to allow for cleavage of all conjugates from the particle surface. We still considered this result as promising for the planned surface-based studies, as the local concentration of MMPs should be significantly higher in the immediate vicinity of the cells.

2.4. Release Studies

As a model substance for cargo release, we selected the proapoptotic peptide KLA (sequence: RRRRRRGGKLA₂KLAKLAKLAKLAK, molecular weight 2.7 kDa),^[18] which was synthesized

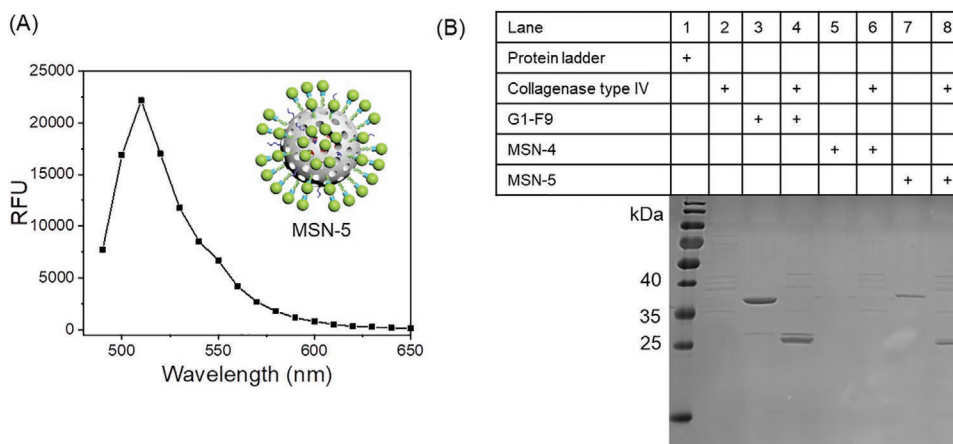


Figure 4. Characterization of MSN-5. A) The representative emission spectrum of MSN-5 using an excitation wavelength of 460 nm. B) 16% SDS-PAGE analysis of MSN-5 treated with or lacking collagenase type IV.

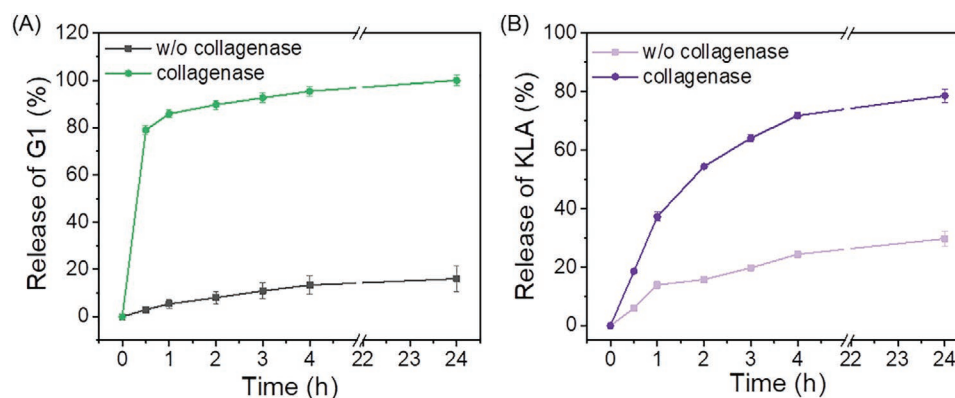


Figure 5. Release of A) G1 protein and B) Cy3-labeled KLA from MSN-6@G1-F9 under acidic conditions at pH 5.3.

using Fmoc-solid phase peptide synthesis method and labeled with a Cy3 dye at the N-terminus. Initial release studies were carried out in homogeneous solution. To this end, the model cargo KLA was sonicated with MSN-4 for 15 min, followed by incubation at room temperature overnight before pore sealing was achieved by incubation with GX-F9 (see Figure 3). After removal of excess GX-F9 by washing the particles with buffer, the loading capacity of KLA was calculated to be $15.7 \pm 2.1 \mu\text{g mg}^{-1}$. The cargo-loaded particles (denoted as MSN-6@GX-F9, see Figure 3) were then subjected to collagenase IV (final concentration: 0.5 mg mL^{-1} , see Figure S18 in the Supporting Information) treatment and the released KLA was monitored by fluorescence spectroscopy at variable time points.

We observed that KLA could not be released from MSN-6@G1-F9 at neutral pH, even in the case of open mesopores (Figure S19, Supporting Information). Presumably, the positive charge of KLA mediates a strong adsorption to the negatively charged MSN surface, similar as previously observed for the release of doxorubicin from aptamer-gated MSNs.^[7] Under acidic conditions, however, $\approx 100\%$ of G1 protein was cleaved, and $\approx 80\%$ of KLA was released from the mesopores in the presence of collagenase IV (Figure 5). By contrast, only $\approx 20\%$ of KLA was released in the absence of collagenase (Figure 5B). Likely, this proportion corresponds to the amount of KLA that is unspecifically adsorbed on the MSN surface and/or embedded in unsealed pores. Nevertheless, the results indicated that the designed MMP-responsive G1-F9-capped MSNs indeed have the appropriate functionality to be used for surface-based cell studies.

2.5. Cell Studies on MSN-Patterned Surfaces

Having shown the basic functioning of the MMP-responsive G1-F9-capped MSNs, we now wanted to exploit the constructs for surface-based cell studies. To this end, we used microcontact printing^[7] to pattern glass substrates with the captured oligonucleotide aF10 that is complementary to the cF10 oligomer attached to the MSN surface (see Figure 3). These surfaces were then used for immobilization of MSNs. In initial experiments, we investigated the adhesion of HT1080 cells on line patterns decorated with MSN-4 (containing cF9 and cF10 oligonucleotides, see Figure 3). HT1080 cells were then seeded on

MSN-4-decorated line patterns and cultured under the standard conditions for 24 h, followed by cell fixation with paraformaldehyde (PFA) and cell staining with Alexa 546-labeled phalloidin and Hoechst 33342. Similar as previously reported for adhesion of MCF7 cells on aptamer-gated MSN patterns,^[7] we found that the majority of HT1080 cells ($\approx 85\%$) adhered to the particle-decorated line patterns (Figure S20, Supporting Information), thus indicating that the particle-decorated surfaces exhibit a greater attractiveness for the cells than the unmodified glass surface.

Next, adhesion of HT1080 cells to patterned substrates decorated with DNA-protein-gatekeeper-capped MSN-5 revealed that $\approx 65\%$ of HT1080 cells preferred to bind on the MSN-5-decorated lines (Figure 6). The somewhat lower selectivity, as compared to MSN-4 surfaces, can be explained by the presence of a protein layer on the MSN-5, which leads to a weakened interaction with the cell membrane, as compared to “naked” DNA-modified particle surfaces that are known to interact strongly with the cell membrane.^[6]

Surprisingly, we also observed that the EGFP fluorescence of G1 was not detectable in the surface-immobilized MSN-5 patterns, presumably due to surface-induced quenching of the EGFP fluorescence (Figure S21, Supporting Information). However, the quenching of EGFP fluorescence was reversible, as indicated in the cell adhesion experiment, wherein various cells on the MSN-5 patterns showed a clear EGFP fluorescence signal in the cytosol (Figure 6C). Since the stable DNA linker in between the particle and the glass surface prohibits cellular uptake,^[6,7] the MSN-5 particles were not ingested by the adhered HT1080 cells (Figure S22, Supporting Information). Therefore, the appearance of the EGFP signal indicated that the G1 protein was cleaved by MMPs secreted by the adhered cells and subsequently ingested by the cells.

To investigate whether incorporated KLA cargo has an influence on cell adhesion and can be released from the surface, HT1080 cells were then seeded on MSN-6-decorated line patterns. To this end, Cy3-labeled KLA (Cy3-KLA) was loaded into the particles, and the resulting particles MSN-6 (Figure 3; for physicochemical characterization, see Table S6 in the Supporting Information) were used for the preparation of the micropatterned surfaces, as described above. Since MSN-6 do not contain the protein gatekeeper, we found that the majority of the cells ($\approx 89\%$) adhered to the MSN-decorated lines (Figure S23, Supporting Information), as it was observed for

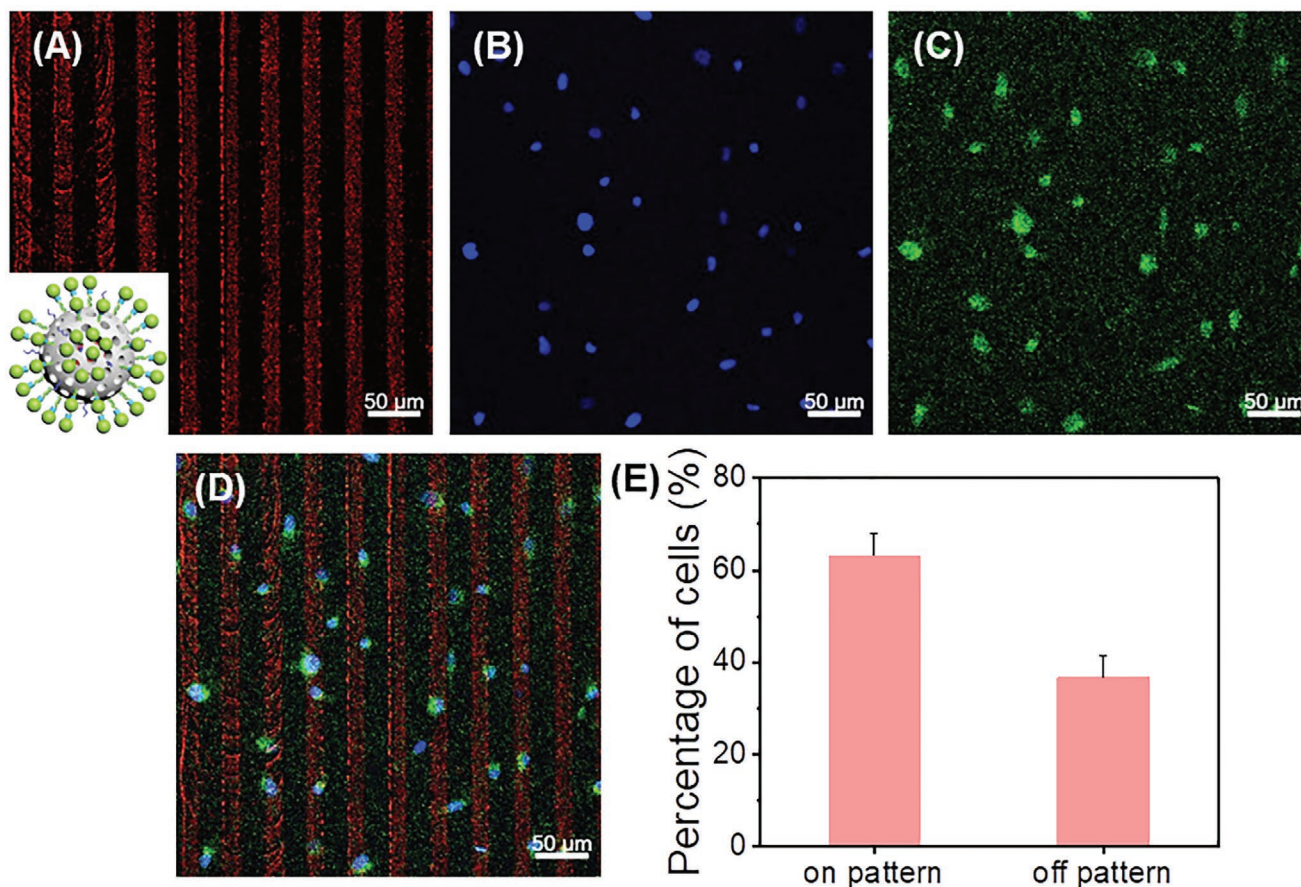


Figure 6. HT1080 cells adhered on an MSN-5-decorated line pattern. A) MSN-5 (red) immobilized on the micropatterned aF10 oligonucleotide lines. B) Cell nuclei (blue) of HT1080 stained with Hoechst 33342. C) EGFP signal (green) of the G1 protein. Note that several cells adhered on the MSN-5 patterns reveal the EGFP fluorescence, thus suggesting that the protein was cleaved by MMPs and ingested by the cells. D) Merge. E) Statistical analysis of cells bound on or off the MSN-5-decorated pattern. Note that $\approx 65\%$ of HT1080 cells preferred to adhere on MSN-5-decorated line patterns ($n = 4$, ≈ 1000 cells were counted).

the purely DNA-modified MSN-4 (Figure 6E). Moreover, a distinctive Cy3 signal appeared in cell's cytosol (Figure S23, Supporting Information), indicating that the Cy3-labeled KLA cargo was released from the particles and taken up by the cells.

To further investigate the functionality of the developed gatekeeper conjugates, HT1080 cells were then seeded on line patterns decorated with KLA-loaded MSN-6@G1-F9 (see Figure 3). After 24 h of incubation, the cells were fixed with PFA and stained to enable microscopy inspection. It is shown in Figure 7 that cells on the lines decorated with the cleavable gatekeeper constructs (MSN-6@G1-F9), revealed the fluorescent signals of both the EGFP of the G1 gatekeeper as well as of Cy3-KLA. This observation clearly indicated the successful cleavage of the gatekeeper from the particle surface, which led to release and uptake of the G1 protein and the Cy3-KLA cargo. By contrast, no intracellular fluorescent signal of EGFP or Cy3-KLA could be observed in the case of the cells adhered to the lines decorated with the uncleavable gatekeeper constructs (MSN-6@G4-F9, see Figure S24 in the Supporting Information). Hence, these results indicated the successful development of MMP-cleavable MSN constructs, which are functional on the solid surface under cell culture conditions.

To test the cytotoxic effect of the KLA-loaded “biopebble containers,” HT1080 cells were seeded on line patterns decorated with MSN-6@G1-F9 that was loaded with unlabeled KLA to prevent interference of the Cy3 label with the fluorescence of propidium iodide (PI). PI staining revealed that about 15% of the cells on the pattern could be identified as dead cells (Figure S25, Supporting Information). This amount was somewhat lower than that observed in control experiments, wherein a homogeneous suspension of MSN-6@G1-F9 was applied to HT1080 cells (about 40% reduction of cell viability, see Figure S26 in the Supporting Information). The relatively low cytotoxicity of KLA is in agreement with the literature,^[18b] indicating that this peptide is nontoxic to the majority of eukaryotic cells' reduction. We attribute the decrease in toxicity observed for the surface-based KLA delivery to the fact that dead cells cannot adhere longer strongly to the solid substrate and thus are washed away during the PI staining process.

Finally, we also confirmed that lines bearing KLA-loaded MSNs, which were capped either with a cleavable (MSN-6@G1-F9) or a noncleavable gatekeeper (MSN-6@G4-F9), have a significant effect on HT1080 cell adhesion. To demonstrate this in a

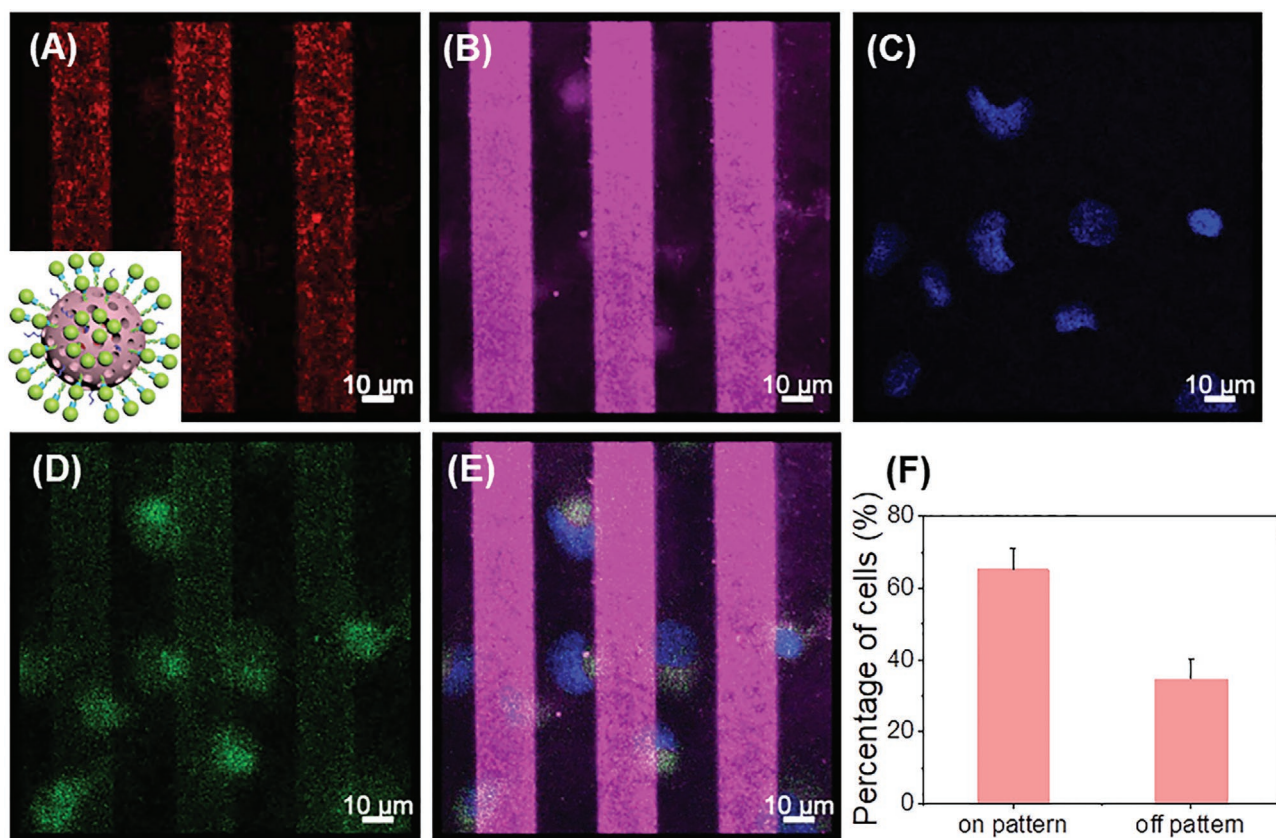


Figure 7. Representative fluorescence microscopy images of HT1080 cells adhered onto KLA-loaded MSN-6@G1-F9-decorated line patterns. A) Cy5 fluorescence (red) of MSN-6@G1-F9. B) Cy3-KLA (magenta). C) Cell nuclei of Hoechst 33342-stained HT1080 cells. D) EGFP fluorescence (green) of the released G1 gatekeeper in the cytosol of the cells. E) Merge. F) Statistical analysis of cells bound on or off the MSN-6@G1-F9-decorated line patterns. Note that $\approx 65\%$ of HT1080 cells adhered to the MSN-6@G1-F9-decorated line patterns ($n = 4$, ≈ 600 cells were counted).

single experiment, we used cross-patterned lines on which either MSNs with the cleavable or noncleavable gatekeeper were immobilized using orthogonal DNA hybridization (Figures S27 and S28, Supporting Information). The results clearly showed that the immobilization of the two different DNA oligonucleotides used for this purpose led to no differences in cell adhesion (Figure S27, Supporting Information). However, the presence of a cleavable or noncleavable gatekeeper caused a significant $\approx 1:2$ difference in the number of cells growing on KLA-loaded MSN-6@G1-F9 or MSN-6@G4-F9, respectively (Figure S28, Supporting Information).

This drastic decrease in cells on lines decorated with KLA-loaded MSNs equipped with cleavable gatekeepers clearly indicates that the cell-triggered release of the cytotoxic agent leads to highly localized concentrations able to primarily affect the cells in close contact with the particles. For adjacent cells that are separated only by a distance of a few micrometers and that are growing on MSNs where the release of the cytotoxic peptide is hindered by the noncleavable gatekeeper system, the local concentration of KLA is substantially lower, which manifests in the higher cell count. The attractiveness of MSNs for cell adhesion in combination with the highly localized delivery of active agents makes the described system a well-suited tool for studying the interaction of various cells and tissues with bioactive surfaces.

3. Conclusions

In summary, we here reported on the development of a cell-responsive biohybrid interface that can be used for spatially confined release of molecular cargo. By taking full advantage of the highly specific Watson-Crick base pairing of complementary DNA oligonucleotides, we designed a bottom-up approach for the DNA-directed assembly of protein-gated MSNs and their DNA-mediated immobilization on microstructured surface patterns. Of particular importance is the enormously high modularity of the system presented here. On the one hand, any other DNA-protein gatekeeper conjugates can be used instead of the EGFP used here for sealing the mesopores of the MSNs. For example, by incorporating specific recognition peptides, other proteases secreted by cells can be used as effectors for the release of the encapsulated cargo, or other bulky proteins can be made available for uptake into the cytosol by cell-based cleavage. On the other hand, orthogonally addressable oligonucleotides can be installed on the MSN surface and harnessed to achieve site-specific immobilization on solid substrates. This allows the production of multicolored surface patterns on planar glass surfaces, as shown in this work. Another advantage of the system described here stems from the unique properties of DNA linkers. While DNA can be degraded by a variety of nucleases, we have not

observed this process unintentionally in any of our previous studies of DNA-directed assembly of proteins and nanoparticles.^[19] The stability of the system is also clearly evident in the present study, as the DNA linker shows sufficient stability, even under cell culture conditions, to prevent cleavage of the particles from the surface and subsequent cellular uptake (see, e.g., Figure S22 in the Supporting Information). On the other hand, sequence features can be specifically incorporated into the linkers to induce cleavage in a targeted manner and thus enable release of surface immobilized components. It should also be possible to integrate such MSN constructs by hybridization into soft 3D DNA materials, such as DNA-based hydrogels and composite materials.^[20] In addition, the DNA-based assembly system offers the possibility to couple the responsive MSN constructs with complex functional nanostructured ligand arrangements to create bioinstructive material systems applicable for cell culture, tissue engineering, or other areas of nanobiotechnology.

Supporting Information

Supporting Information is available from the Wiley Online Library or from the author.

Acknowledgements

This work was financially supported through the Helmholtz program “Materials Systems Engineering” under the topic “Adaptive and Bioinstructive Materials Systems”. P. Sun acknowledges China Scholarship Council (CSC) for financial support of her Ph.D. studies at KIT.

Open access funding enabled and organized by Projekt DEAL.

Conflict of Interest

The authors declare no conflict of interest.

Data Availability Statement

Research data are not shared.

Keywords

bioanotechnology, cell-responsive interfaces, DNA-directed assembly, DNA–protein conjugates, mesoporous particles

Received: October 29, 2020

Revised: May 6, 2021

Published online:

- [1] a) A. M. Ross, Z. X. Jiang, M. Bastmeyer, J. Lahann, *Small* **2012**, *8*, 336; b) J. Wegener, in *Cell Surface Interactions*, John Wiley & Sons, Inc., New York **2006**; c) T. Satav, J. Huskens, P. Jonkheijm, *Small* **2015**, *11*, 5184.
- [2] K. Zhang, S. Wang, C. Zhou, L. Cheng, X. Gao, X. Xie, J. Sun, H. Wang, M. D. Weir, M. A. Reynolds, N. Zhang, Y. Bai, H. H. K. Xu, *Bone Res.* **2018**, *6*, 31.
- [3] A. D. Celiz, J. G. W. Smith, R. Langer, D. G. Anderson, D. A. Winkler, D. A. Barrett, M. C. Davies, L. E. Young, C. Denning, M. R. Alexander, *Nat. Mater.* **2014**, *13*, 570.
- [4] A. M. Lipski, C. J. Pino, F. R. Haselton, I. W. Chen, V. P. Shastri, *Biomaterials* **2008**, *29*, 3836.
- [5] K. Kang, S. E. Choi, H. S. Jang, W. K. Cho, Y. Nam, I. S. Choi, J. S. Lee, *Angew. Chem., Int. Ed. Engl.* **2012**, *51*, 2855.
- [6] A. Leidner, S. Weigel, J. Bauer, J. Reiber, A. Angelin, M. Grösche, T. Scharnweber, C. M. Niemeyer, *Adv. Funct. Mater.* **2018**, *28*, 1707572.
- [7] P. Sun, A. Leidner, S. Weigel, P. G. Weidler, S. Heissler, T. Scharnweber, C. M. Niemeyer, *Small* **2019**, *15*, e1900083.
- [8] a) R. P. Verma, C. Hansch, *Bioorg. Med. Chem.* **2007**, *15*, 2223; b) G. Shay, C. C. Lynch, B. Fingleton, *Matrix Biol.* **2015**, *44–46*, 200.
- [9] a) H. Sato, T. Takino, Y. Okada, J. Cao, A. Shinagawa, E. Yamamoto, M. Seiki, *Nature* **1994**, *370*, 61; b) M. W. Roomi, J. C. Monterey, T. Kalinovsky, M. Rath, A. Niedzwiecki, *Oncol. Rep.* **2009**, *21*, 1323.
- [10] a) J. J. Liu, B. L. Zhang, Z. Luo, X. W. Ding, J. H. Li, L. L. Dai, J. Zhou, X. J. Zhao, J. Y. Ye, K. Y. Cai, *Nanoscale* **2015**, *7*, 3614; b) G. Zhu, L. Meng, M. Ye, L. Yang, K. Sefah, M. B. O'Donoghue, Y. Chen, X. Xiong, J. Huang, E. Song, *Chem. - Asian J.* **2012**, *7*, 1630.
- [11] V. Lapiene, F. Kukolka, K. Kiko, A. Arndt, C. M. Niemeyer, *Bioconjugate Chem.* **2010**, *21*, 921.
- [12] a) P. A. Elkins, Y. S. Ho, W. W. Smith, C. A. Janson, K. J. D'Alessio, M. S. McQueney, M. D. Cummings, A. M. Romanic, *Acta Crystallogr., Sect. D: Biol. Crystallogr.* **2002**, *58*, 1182; b) G. Rosenblum, P. E. Van den Steen, S. R. Cohen, J. G. Grossmann, J. Frenkel, R. Sertchook, N. Slack, R. W. Strange, G. Opendakker, I. Sagi, *Structure* **2007**, *15*, 1227.
- [13] G. Dhar, E. R. Sanders, R. C. Johnson, *Cell* **2004**, *119*, 33.
- [14] F. Kukolka, C. M. Niemeyer, *Org. Biomol. Chem.* **2004**, *2*, 2203.
- [15] Y. Soini, T. Hurskainen, M. Hoyhtya, A. Oikarinen, H. Autio-Harmainen, *J. Histochem. Cytochem.* **1994**, *42*, 945.
- [16] a) J. Zhang, X. Li, J. M. Rosenholm, H.-c. Gu, *J. Colloid Interface Sci.* **2011**, *361*, 16; b) J. Gu, K. Huang, X. Zhu, Y. Li, J. Wei, W. Zhao, C. Liu, J. Shi, *J. Colloid Interface Sci.* **2013**, *407*, 236.
- [17] T. Myochin, K. Hanaoka, T. Komatsu, T. Terai, T. Nagano, *J. Am. Chem. Soc.* **2012**, *134*, 13730.
- [18] a) B. Law, L. Quinti, Y. D. Choi, R. Weissleder, C. H. Tung, *Mol. Cancer Ther.* **2006**, *5*, 1944; b) I. D. Alves, M. Carré, M.-P. Montero, S. Castano, S. Lecomte, R. Marquant, P. Lecorché, F. Burlina, C. Schatz, S. Sagan, G. Chassaing, D. Braguer, S. Lavielle, *Biochim. Biophys. Acta, Biomembr.* **2014**, *1838*, 2087.
- [19] a) C. M. Niemeyer, *Angew. Chem., Int. Ed.* **2010**, *49*, 1200; b) R. Meyer, S. Giselsbrecht, B. E. Rapp, M. Hirtz, C. M. Niemeyer, *Curr. Opin. Chem. Biol.* **2014**, *18C*, 8.
- [20] Y. Hu, C. M. Domínguez, S. Christ, C. M. Niemeyer, *Angew. Chem., Int. Ed.* **2020**, *59*, 19016.